STORM ANALYSIS USING TENSOR FIELD VISUALIZATION

Alexandra Naegele[1], Raymundo Navarrete[2], and Andrew Zdyrski[3]

Abstract. Reconstructed global atmospheric data sets have the potential to provide information about major storm events that can be related to ground observations through visualization of atmospheric dynamics. The evolution of a storm event over time has traditionally been analyzed using direct analysis of the velocity vector field, but this method cannot be easily used to study the storms spatial characteristics at a given time. In order to analyze the structure of storms more efficiently, cross-sections along chosen pressure levels of a storm's velocity vector field are used to generate velocity gradients, that is, asymmetric tensor fields that describe spatial characteristics of a vector field. In order to simplify analysis of a storm's velocity gradient, we integrated atmospheric science concepts, mathematical transformations, and computer visualization techniques (tensor field visualization techniques) to represent important storm characteristics, such as anisotropic stretching and the relative proportions of isotropic scaling and rotation. These visualization techniques were used to represent the structure of velocity fields in wind data at the 1000, 7000, 400 and 100 millibar heights across the eastern Pacific at 6-hour time intervals for a 2-week period that produced a record flood event in 1996 in the Willamette Valley, Oregon. Additionally, a set of transformations was developed and implemented to visualize the storms velocity gradient relative to non-stationary frames of reference. The visualizations provide information about the movement and strength of air masses and provide a basis to assess the agreement between global reconstructed data sets and ground observations during this unusual event.

[1]Environmental Science, Ohio State University, Columbus, OH, USA
[2]Mathematics and Engineering Physics, University of Arizona, Tucson, AZ, USA
[3]Computer Science, University of Hawaii, Hilo, HI, USA

Introduction

It goes without saying that the study of storm events not only has many important applications but is also necessary for the well being of our communities, especially those that are likely to experience strong meteorological events. For this reason, basic storm analysis techniques have existed since the development of modern meteorology. Nonetheless, thanks to the increase in awareness of the reality of global climate change and its effects on the frequency and power of storms, it is now apparent that more sophisticated techniques are necessary to fully understand storms, their effects on our environment, and how global climate change is affecting them.

A new approach in the study of storms that may be fruitful applies recently developed asymmetric tensor field visualization techniques [1] to study the vector field produced by a storm at a given time. This technique consists of obtaining longitudinal and latitudinal velocities of a storm at different points at a given time and along a given altitude to create a two-dimensional velocity vector field of the storm, which is then used to create its corresponding velocity gradient (a special asymmetric tensor field as will be explained shortly). Asymmetric tensor field visualization techniques are then used to visualize important characteristics of the velocity gradient (and the storm) such as the degree at which the storm is expanding, rotating, and stretching at each point. Consequently, this form of analysis can explain the storm's spatial structure at a given time and can be used to relate global reconstructed data sets of a storm to ground observations, which may be helpful in determining whether the structure of storms has been changing over the years due to global climate change.

The purpose of this paper is to present the results we obtained when we applied the new visualization techniques to storm analysis. In the following sections we will explain exactly what type of data was used for the analysis, how the vector and tensor fields were obtained, how the distortion coefficients of the storm (expansion, rotation, stretching) are calculated, how the visualization is computed, and what our results were.

Finally, in order to test the new techniques, the Willamette Valley Flood of 1996, a significant historical meteorological event that occurred in Oregon, was chosen to apply our analysis. This flood was the result of a series of low-pressure systems whose effects were felt throughout Oregon from February 1-14, 1996, and was part of a larger series of floods which spanned the entire Pacific Northwest. These low-pressure air masses originated in the sub-tropical Pacific region and flowed northward where they eventually transformed into mid-latitude cyclones. The precipitation was greatest during the period from February 5-9, peaking at 9 mm/hr on both February 7 and February 9, which corresponds to the flooding which peaked on February 7 (Perkins and Jones). The intensity of the precipitation in combination with the existing snowpack resulted in severely damaging high streamflow and flooding.

1. Storms and Tensor Fields

In order to understand how the visualization works and what it can do for us, it is important to have an idea of the structure of the data used and how it is used to create the gradient velocity tensor fields of a storm. Therefore, section 1.1 contains an explanation of the kind of data that we were dealing with, while section 1.2 explains the mathematics necessary to understand the visualization.

1.1. **Data Structure.** The data used for the visualization was from the NCEP-DOE Reanalysis 2 dataset. This is a freely available dataset from the National Center for Environmental Prediction. The data is generated from global forecast models in addition to observed weather readings. The dataset timeline is from 1979 to 2008, with measurements available every 6 hours. For our purposes, a timeframe beginning at January 26, 1996 to February 9, 1996 was used to show the storm(s) that resulted in the 1996 flood of the Willamette Valley. There are many different types of data available in the dataset, such as wind speed, geopotential height, air temperature, and relative humidity. We were concerned with wind speed in both the latitudinal and longitudinal direction.

The resolution of the data, that is to say the physical distance between each data point, is 2.5 degrees in latitude and longitude. The area that we wished to visualize was a rectangle whose bottom left corner was 180.0E, 0.0N and the top right corner was 242.5E, 47.5N. This gave us a grid with dimensions 20 by 26 where each point on the grid contained a vertical and horizontal wind component.

The dataset has many different types of data, including wind speed, for varying pressure levels. The pressure levels correspond to different altitudes in the atmosphere. In order to visualize the series of storms at different heights, four different pressure levels were used as shown (Table 1).

Table 1. Altitudes corresponding to different pressure levels.

Pressure [hPa]	Altitude [m]
1,000	0 (surface)
700	3,000
400	7,200
100	16,200

Each pressure level defines a different 20 by 26 grid with different wind speeds at each point.

The NCEP-DOE Reanalysis data is available only in NetCDF format, which are binary files. In order to make the files suitable for reading into a program, we first

had to convert them to a text format. This was done using the NetCDF Operators (NCO) tools (available at http://nco.sourceforge.net) to convert the binary data files to text files. After the text files were created, it was decided the most useful format for the data to be in was a comma separated values (CSV) format. A parsing routine was written for this purpose. The CSV files were then used to create vector field plots in the R programming language and calculate the tensor field in the visualization software.

1.2. **The Velocity Gradient of a Storm.** Once the velocity vector fields of interest are obtain (as described in section 1.1), these are used to calculate the corresponding velocity gradients: tensor fields that contain the spatial derivates of the vector components at each point of the vector field (see section 1.2.1). Since calculating the velocity gradient of each vector field requires taking derivatives along the latitudinal and longitudinal directions of the vector field, special numerical methods were used in order to reduce the error due to the small resolution of our data sets (see section 1.2.2). The reason for calculating the tensor fields of the storm is that these can be used to calculate the coefficients of spatial distortion at each point in space (see section 1.2.3), which are then used to better understand the behavior of the storm at a given time.

1.2.1. *Definition of the Velocity Gradient.* In order to define the velocity gradient of a two-dimensional vector field, we'll introduce the following mathematical objects:

Let $\mathbf{r}(x,y) = \begin{pmatrix} x \\ y \end{pmatrix}$ represent the standard position coordinates of $\mathbb{R}^2$ and let $\mathbf{v} : \mathbb{R}^2 \to \mathbb{R}^2$, $\mathbf{v}(\mathbf{r}) = \begin{pmatrix} v_x(\mathbf{r}) \\ v_y(\mathbf{r}) \end{pmatrix}$ be a vector field from $\mathbb{R}^2$ to $\mathbb{R}^2$. Also, let $\nabla = (\partial_x \ \partial_y)$ denote the gradient vector and $\otimes$ denote the tensor product.

When applied to our storm tracking analysis, x and y represent the longitudinal and latitudinal angular distances from a given reference point (since only a small portion of Earth's surface is considered, we can treat it as a plane subset of $\mathbb{R}^2$). Correspondingly, $\mathbf{r}$ is the position vector from the chosen reference point. Finally, $\mathbf{v}(\mathbf{r})$ represents the surface velocity vector field of the storm, which contains the longitudinal and latitudinal velocities at each point.

The velocity gradient of $\mathbf{v}(\mathbf{r})$ is defined as

$$J(\mathbf{r}) = \nabla \otimes \mathbf{v}(\mathbf{r}) = \begin{pmatrix} \partial_x v_x(\mathbf{r}) & \partial_y v_x(\mathbf{r}) \\ \partial_x v_y(\mathbf{r}) & \partial_y v_y(\mathbf{r}) \end{pmatrix}$$

Then, $J(\mathbf{r})$ is a second order tensor field defined in $\mathbb{R}^2$ which contains the spatial derivatives of each component of the vector field $\mathbf{v}(\mathbf{r})$. This information is all we need to understand how a vector field (or a storm) changes in any direction, and as it will be shown, it can also be used to measure the distortion of the storm at each point.

1.2.2. *Obtaining the Velocity Gradient Numerically.* Since the data available for the velocity vector field at the location of interest consists of a 20 by 26 set of points equally separated by 2.5 degrees, the numerical spatial derivatives that are part of the tensor field can be obtained using simple two-point differentiation. Nonetheless, due to the small resolution of the data set, using finite difference approximations is not the best approach. Instead, a higher order method that uses a 5 by 5 grid centered at each point to calculate its spatial derivatives was used (finite difference approximations were used for the points in the edges that do not have a 5 by 5 window around them).

The higher order method used for the differentiations is a variation of the five-point stencil method: For a function $f(x)$ and constant $h > 0$, $f'(x)$ is given by

$$f'(x) = \frac{-f(x+2h) + 8f(x+h) - 8f(x-h) + f(x-2h)}{12h}$$

In two dimensions, this method can be used to obtain the two spatial derivatives of each vector field component (just replace f by v_1 and v_2 and repeat for y), but in order to take full advantage of the 5 by 5 window around each point, the same spatial derivatives were calculating using the five-point stencil method this time along the diagonals of the 5 by 5 window (which can be used to calculate the derivatives of interest), and finally a weighted average yielded the desired results.

1.2.3. *Calculating the Coefficients of Spatial Distortion.* Once the gradient velocity $J(\mathbf{r})$ of the storm's vector field is calculated, we can then calculate the coefficients of spatial distortion that we wish to visualize. For a given tensor field $J(\mathbf{r}) = \begin{pmatrix} T_{11}(\mathbf{r}) & T_{12}(\mathbf{r}) \\ T_{21}(\mathbf{r}) & T_{22}(\mathbf{r}) \end{pmatrix}$:

1) The coefficient of isotropic scaling $\gamma_d(\mathbf{r})$ (which measures the degree at which fluid flow due to the vector field is likely to expand or contract at a given point) is given by

$$\gamma_d(\mathbf{r}) = \frac{T_{11}(\mathbf{r}) + T_{22}(\mathbf{r})}{2}$$

2) The coefficient of rotation $\gamma_r(\mathbf{r})$ (which measures the degree at which fluid flow due to the vector field is likely to rotate) is given by

$$\gamma_d(\mathbf{r}) = \frac{T_{21}(\mathbf{r}) - T_{12}(\mathbf{r})}{2}$$

3) The coefficient of anisotropic stretching $\gamma_s(\mathbf{r})$ (which measures the degree at which fluid flow due to the vector field is likely to move along one direction over the others) is given by

$$\gamma_s(\mathbf{r}) = \frac{\sqrt{(T_{11}(\mathbf{r}) - T_{22}(\mathbf{r}))^2 + (T_{12}(\mathbf{r}) + T_{21}(\mathbf{r}))^2}}{2}$$

Figure 1 shows examples of three vector fields whose tensor field is constant and that only have one non-zero coefficient of spatial distortion (one for each coefficient). It is important to remember though that the coefficients can vary from point to point and that more than one nonzero coefficient can be present at one point in the vector field.

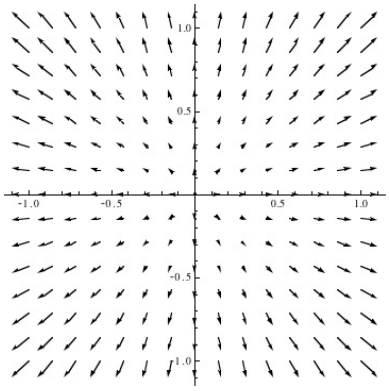

$$\mathbf{v}(x,y) = \begin{pmatrix} x \\ y \end{pmatrix}$$
$$T(x,y) = \begin{pmatrix} 1 & 0 \\ 0 & 1 \end{pmatrix}$$
$$\gamma_d = 1$$
$$\gamma_r = 0$$
$$\gamma_s = 0$$

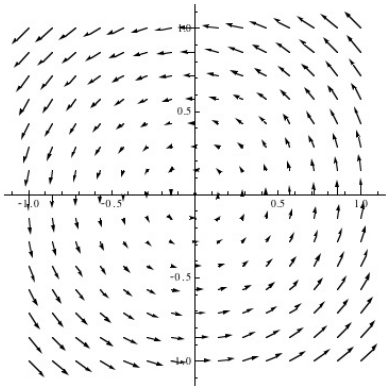

$$\mathbf{v}(x,y) = \begin{pmatrix} -y \\ x \end{pmatrix}$$
$$T(x,y) = \begin{pmatrix} 0 & -1 \\ 1 & 0 \end{pmatrix}$$
$$\gamma_d = 0$$
$$\gamma_r = 1$$
$$\gamma_s = 0$$

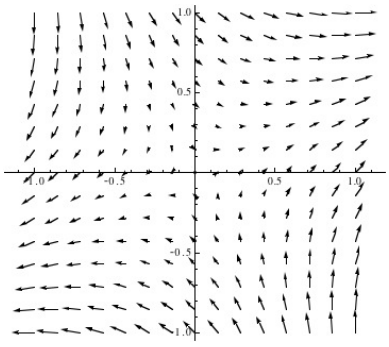

$$\mathbf{v}(x,y) = \begin{pmatrix} x+y \\ x-y \end{pmatrix}$$
$$T(x,y) = \begin{pmatrix} 1 & 1 \\ 1 & -1 \end{pmatrix}$$
$$\gamma_d = 0$$
$$\gamma_r = 0$$
$$\gamma_s = \sqrt{2}$$
$$\theta = \pi/2$$

FIGURE 1. Examples of vector fields with only one nonzero constant coefficient of distortion. Any vector field can be depicted as a combination of these coefficients of distortion.

2. The Asymmetric Tensor Field Visualization Technique

Once the velocity gradient of a storm and its coefficients of spatial distortion at each point are known, it is only necessary to decide how each coefficient will be represented in the visualization. This section provides an explanation of what the visualizations represent (see section 2.1) and how these are obtained (see section 2.2).

2.1. **Understanding the Visualization.** For each point of the velocity field, the corresponding tensor was decomposed into three coefficients of spatial distortion: isotropic scaling, rotation, and anisotropic stretching. From this decomposition, a block of color could be associated with each particular point. Specifically, the hue was determined as a ratio between the isotropic scaling and rotation. For pure isotropic scaling in both the positive and negative directions, and clockwise and counter-clockwise rotation, a specific color was assigned (Figure 2). For all combinations of rotation and isotropic scaling then, a specific hue was assigned based on the ratio of the two components. To account for the amount of anisotropic stretching, variable transparency was used. Unlike the other two components, anisotropic stretching was computed separately, by dividing the amount of stretching at each point by the maximum stretching throughout the entire field at the given time frame. Therefore, as the ratio increases, the more transparent the shade becomes.

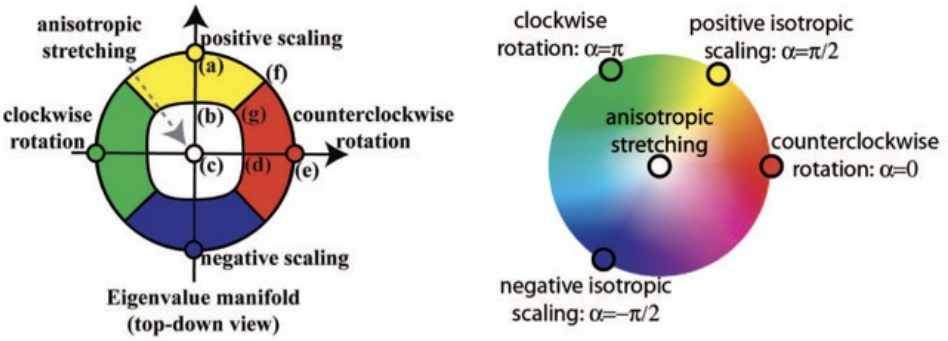

Figure 2. Coloring Scheme: The relative ratio between isotropic scaling and rotation is depicted by the hue used while the presence of anisotropic stretching is depicted by the transparency used.

2.2. **Creating the Visualization.** The tensor field visualization was created using two separate programming components. First, the R programming language was used to generate velocity vector plots. Then, C++ with OpenGL was used to calculate the tensor field and overlay the coloring scheme on the velocity vector plots.

The R programming language is a popular language choice for statisticians due to its included statistical and graphical functions. We used R for its plotting routines to generate velocity vector plots for each 6 hour time frame. This was done for the 4

different pressure levels of interest, resulting in 56 plots for each pressure level. A plot is shown below.

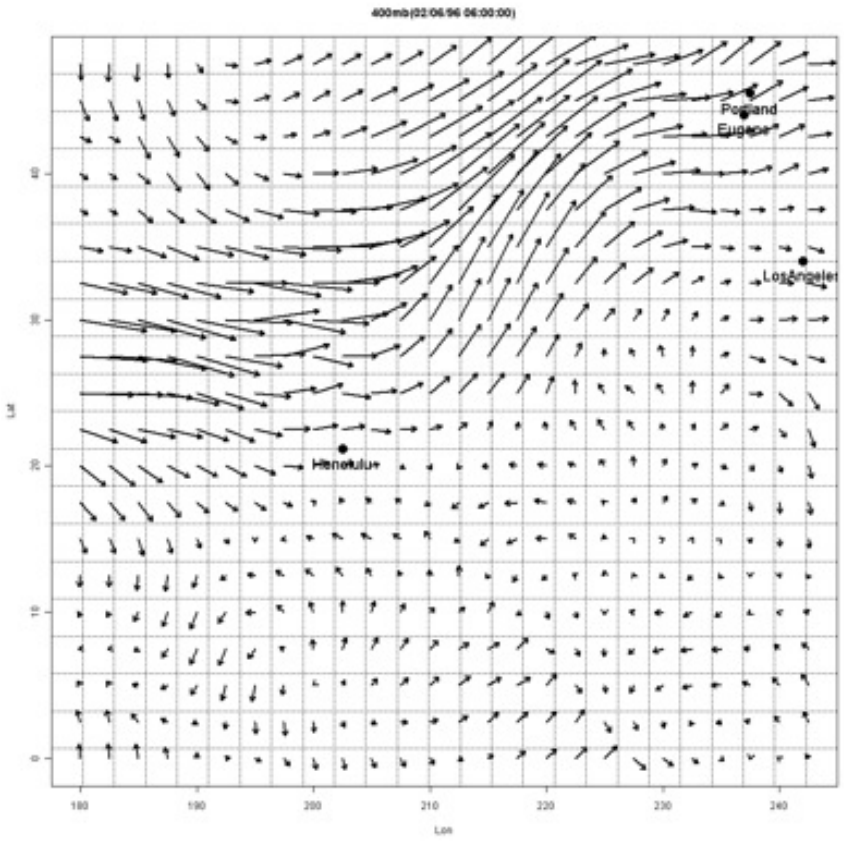

FIGURE 3. Example of a vector field of the storm under analysis.

Each arrow shown in the plot is a velocity vector; the length of the vector denotes its relative magnitude. R was also used to add the location of landmark cities to the plots in order to more clearly see where storms are passing over. Each of these plots was generated as bitmap file to be loaded into the visualization software.

The visualization software had two main tasks. First, the tensor field and decompositions had to be computed from the velocity vector field. Second, the decomposition coloring scheme had to be overlaid on the velocity vector plots. To compute the tensor field and decomposition of the tensors, the CSV files are read in and the horizontal and vertical wind magnitudes are stored in an internal 2 dimensional array. For each element of the array, a tensor is computed in one of three different ways depending on its position within the array. For elements on the boundary of the array or within one position of the boundary, adjacent elements are used to compute the tensor. For the other elements that lie two or more positions within the boundary, elements up to

two positions away are used to compute the tensor. The decomposition which relate to the spatial distortion of a storm is computed from the tensor. The C++ programming language was used to perform these calculations.

The visualization of the decomposition from the tensor field was done using OpenGL. The velocity vector plots (in bitmap format) were read into the visualization software and displayed as a background image. On top of the velocity vector plot, the coloring scheme was drawn on each element of the grid using a colored, transparent rectangle. The color and transparency of the rectangle was related to the decomposition of the tensor, which again is tied to the spatial distortion of a storm (see Figure 4).

To allow the user to control which 6 hour interval and pressure level they are viewing, a simple user interface was created. This was done using GLUI, a library using OpenGL to create user interfaces. A legend is also displayed in the visualization to quickly show the user what atmospheric event each color denotes.

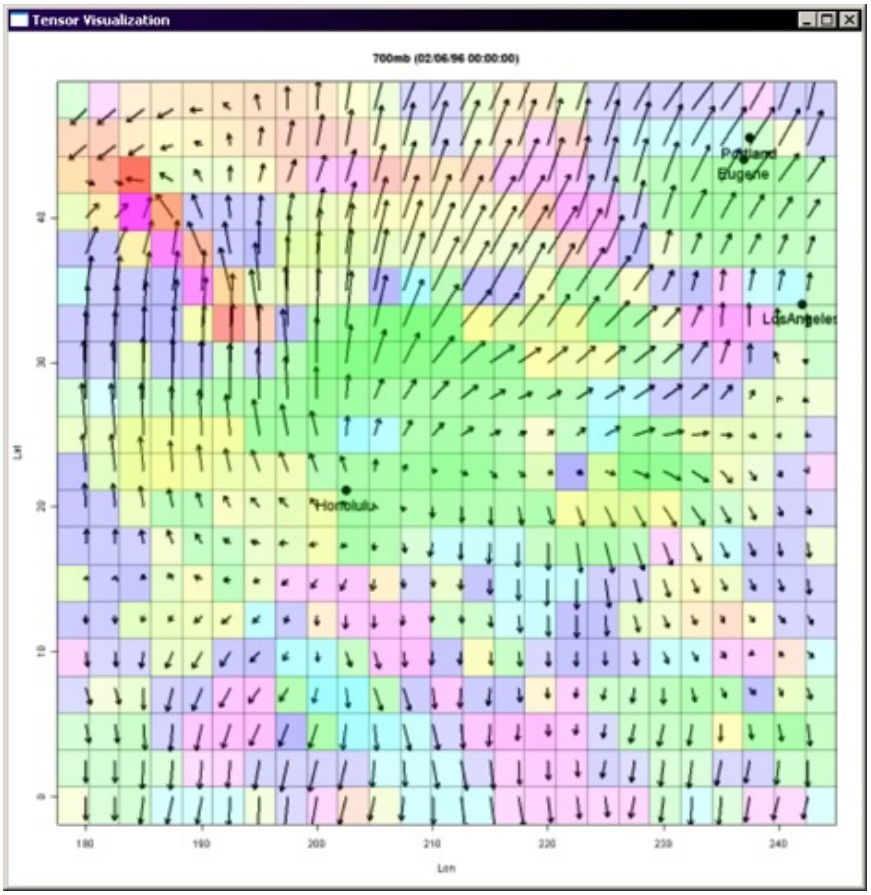

FIGURE 4. Example of the visualization for one of the tensor fields.

3. Conclusions

The purpose of this section is to present an analysis of the usefulness of the visualization techniques when applied to storm analysis (see section 3.1) and to talk about the future work that can be done to fully develop the visualizations (see section 3.2).

3.1. **Interpretation of a Storm's Visualization.** We were able to use this visualization to further understand atmospheric dynamics by identifying the relationship between various components of spatial distortion. Different types of weather systems can be recognized by their method of movement. For example, a low pressure system is often associated with cyclogenesis, especially in the mid-latitude regions. In the northern hemisphere, a cyclone is characterized by counter-clockwise rotation in combination with winds converging at the Earth's surface, which spiral upward to diverge at a higher elevation. Inversely, an anti-cyclone in the northern hemisphere is characterized by clockwise rotation in combination with converging winds at a higher elevation which sink and eventually diverge at the surface level (see Figure 5). Our visualization becomes useful when there is a need to identify storm systems or atmospheric dynamics in general.

Also, by looking at the level of transparency, it is possible to tell whether or not a specific air mass is mostly stationary, or if it is moving. In another example, an air mass that is largely characterized by zonal flow will have high anisotropic stretching, and therefore will be highly transparent. One observation from the visualization has shown that areas with larger coefficients of anisotropic stretching tend to have lower wind magnitudes. It is important, however, to remember that a bolder color does not necessarily correspond with a higher degree of rotation and/or isotropic scaling, only that there exists a small amount of anisotropic stretching resulting from that point's resultant tensor.

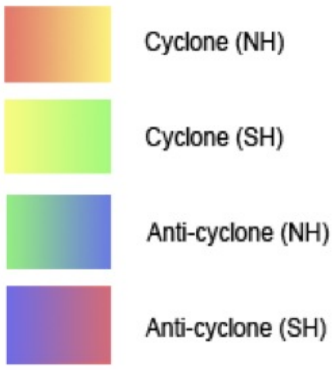

Figure 5. Expected colors for different storm phenomena.

One of the goals of this project was to follow the path of the storm from its origin, and to see whether our visualization corresponded with recorded weather data at the H.J. Andrews Experimental Research Forest. During the peak of the storm, the precipitation data was compared to the corresponding frames of the visualization. Because of the 6 hour time step, we were able to make comparisons to hourly data. For the most part, we were able to detect a low pressure system moving in waves across the H.J. Andrews during the peak of the event. This pattern of the storm system moving in repeated waves was evident as it moved across the Pacific Ocean, and continued as it reached the coast. While the data does not match up perfectly to the visualization, it is likely that the discrepancy is a result of the reconstructed data-set, and more significantly, that the data was taken at such a coarse scale.

3.2. **Future Work.** In the future, several improvements can be made to the visualization, and it can be taken in many directions:

Initially, the area of interest that was decided upon reached only to the northeast corner of Oregon, expecting that that would allow for ample buffer room when analyzing the path of the storm. However, as we progressed with our project, our method of derivation of the tensor field used the five adjacent points in each direction, and as a result the points near the border of our region of interest (of which H.J. Andrews was included) had to undergo a modified version of the differentiation. Therefore, one change that could be added in the future would be to apply the analysis to a larger area of interest, with an appropriately sized buffer along the perimeter.

Additionally, further work on this visualization that would yield greater interpretation would be to include the winds in the z-direction (pointing out radially from the center of the earth). In our visualization, only two dimensions were considered, and including the third dimension would allow us to see movement in the vertical direction as well. This would be especially useful when looking at areas identified by cyclonic and anti-cyclonic motion, as this would allow for study of how the air is rising or falling.

Another direction which could be taken with the visualization created would be to include the eigenvalues and eigenvectors that can be calculated from each tensor as defined in [1]. Due to time restraints, we chose not to visualize the eigenvalue and eigenvector manifolds, but this could yield interesting conclusions about the magnitude of the spatial distortion if completed.

4. Additional Work

In this section we present additional work done during the summer.

4.1. **Vector and Tensor Field Transformations.** The question that we wish to answer with this additional work is: How do the vector and tensor fields of a storm (and consequently its visualization) change when the storm is observed in a non-stationary frame of reference? In other words, how would an observer moving along any given path perceive the properties of a storm? For example, instead of looking at the vector and tensor field visualizations of a storm as these are measure with respect to the earth, it would be interesting to look at these the way an observer moving along with the center of the storm would see them. Our goal was then to develop a set of transformations that can be used to rewrite any position, velocity, and tensor measured in our stationary frame of reference into the ones that would be observed in a difference reference frame. Since the mathematical details of how these transformations were obtained are somewhat heavy, only the results and the consequences will be presented here (see Appendix A for the mathematical details).

We start by restating the position, velocity, and tensor fields already introduced in Section 2.2, but this time with a small change in our notation:

Let S_o represent a stationary frame of reference in a two-dimensional space. Any position observed in S_o can be written in terms of $\{\mathbf{e_1}, \mathbf{e_2}\}$, where $\mathbf{e_1} = \binom{1}{0}$ and $\mathbf{e_2} = \binom{0}{1}$ form the standard unit basis of $\mathbb{R}^2$. Furthermore, let $\mathbf{r} = r_1\mathbf{e_1} + r_2\mathbf{e_2} = \binom{r_1}{r_2}$ be any position in S_o and let $t \in \mathbb{R}$ represent a time parameter. This allows us to define

$$\mathbf{v}(\mathbf{r}, t) = \begin{pmatrix} v_1(\mathbf{r}, t) \\ v_2(\mathbf{r}, t) \end{pmatrix} \qquad \text{and} \qquad J(\mathbf{r}, t) = \begin{pmatrix} \partial v_1(\mathbf{r}, t)/\partial \mathbf{e_1} & \partial v_1(\mathbf{r}, t)/\partial \mathbf{e_2} \\ \partial v_2(\mathbf{r}, t)/\partial \mathbf{e_1} & \partial v_2(\mathbf{r}, t)/\partial \mathbf{e_2} \end{pmatrix}$$

as a vector field and its corresponding tensor field in $\mathbb{R}^2$ as observed in S_o.

Note that these are the same as those defined in section 2.2, just replace $\mathbf{e_1}$ and $\mathbf{e_2}$ with x and y and add a time parameter to the vector and tensor fields.

Next, we'll mathematically define the moving frame in which we wish to visualize the storms vector and tensor fields:

Let $S_t(t) = S_t$ represent a moving frame also in $\mathbb{R}^2$, with an origin positioned at $\mathbf{a}(t) \in \mathbb{R}^2$ with respect to S_o and moving at a velocity $\mathbf{a}'(t) \in \mathbb{R}^2$ with respect to S_o. Any position observed in S_t is written in terms of $\{\mathbf{T}(t), \mathbf{N}(t)\}$, where $\mathbf{T}(t)$ and $\mathbf{N}(t)$ form an orthonormal basis of $\mathbb{R}^2$ and are given by

$$\mathbf{T}(t) = \frac{\mathbf{a}'(t)}{\|\mathbf{a}'(t)\|} \qquad \text{and} \qquad \mathbf{N}(t) = \begin{pmatrix} 0 & -1 \\ 1 & 0 \end{pmatrix} \mathbf{T}(t)$$

Note that $\mathbf{a}$ represents the position of our moving observer as a function of time (with respect to the stationary frame), $\mathbf{a}'$ represents the observer's velocity, and $\mathbf{T}$ and $\mathbf{N}$ are the new axes that the observes uses to measure lengths, one pointing in the direction of motion and the other perpendicular to it.

The final mathematical object that we must define is the following rotational matrix:

$$L(t) = \begin{pmatrix} \mathbf{e_1} \cdot \mathbf{T}(t) & \mathbf{e_2} \cdot \mathbf{T}(t) \\ \mathbf{e_1} \cdot \mathbf{N}(t) & \mathbf{e_2} \cdot \mathbf{N}(t) \end{pmatrix}$$

(this is the change-of-basis matrix from $\{\mathbf{e_1}, \mathbf{e_2}\}$ to $\{\mathbf{T}(t), \mathbf{N}(t)\}$. Also, since it is orthonormal, its inverse $L(t)^{-1}$ is just its transpose).

The goal was then to develop a set of transformations that can be used to rewrite any position, vector, or tensor in S_o as it is observed in S_t. Here are the results:

A position $\mathbf{r}$ in S_o as it is observed in S_t is given by

$$\mathbf{r}_t = L(t)(\mathbf{r} - \mathbf{a}(t))$$

To go back from a position in S_t to the one in S_o,

$$\mathbf{r} = L(t)^{-1}(\mathbf{r}_t) + \mathbf{a}(t)$$

A velocity $\mathbf{v}(\mathbf{r})$ in S_o as observed in S_t is given by

$$\mathbf{v}_t(\mathbf{r}_t) = L(s)(\mathbf{v}(\mathbf{r}, t)) - \mathbf{a}'(t))$$

And in order to express a velocity $\mathbf{v}_t(\mathbf{r}_t)$ in S_t as it is observed in S_o,

$$\mathbf{v}(\mathbf{r}, t) = L(t)^{-1}(\mathbf{v}_t(\mathbf{r}_t)) + \mathbf{a}'(t)$$

Finally, a tensor $J(\mathbf{r}, t)$ in S_o as observed in S_t is given by

$$J_t(\mathbf{r}_t) = L(t)J(\mathbf{r}, t)L(t)^{-1}$$

and of course to go back we use

$$J(\mathbf{r}, t) = L(t)^{-1}J_t(\mathbf{r}_t)L(t)$$

From these equations we can learn quite a bit:

First, as expected, the way the positions, velocity fields, and tensor fields are expressed in S_o are completely changed when we move to S_t (due to the change basis). The velocity field also goes through further change, since the relative velocities due to the observer's motion have to be taken into account. Again, these are obvious results, what wasn't obvious was how the tensor field would change.

Note that since $L(t)$ and $L(t)^{-1}$ do not depend in the magnitude of $\mathbf{a}'(t)$ (only the direction of motion of S_t is used), $J_t(\mathbf{r}_t)$ depends in the new coordinate system used

but not in the motion of S_t. In other words, the tensor field remains invariant to the transformations (in contrast to the velocity vector field); the transformations only serve to rewrite each tensor in terms of the new coordinate system but do not alter the tensor field. This answers our original question: the way the tensor field is perceived in non-stationary reference frames shouldn't change. This implies that any information obtained about the tensor field of a storm in any reference frame can be directly applied to study the storm in any other reference frame.

The final and most important consequence of these results is that since the transformation leaves the tensor field invariant, the tensor field decompositions remain basically the same. Section A.3 shows that indeed the distortion coefficients γ_d, γ_r, and γ_s do not change after the transformation (the only value that changes is the angle of anisotropic rotation θ, which depends on the orientation of S_t) and therefore the tensor field visualizations do not change (other than being repositioned along with the positions and the transformed velocity field). Therefore, no new visualizations have to be performed when we wish to study a storm in other reference frames, since these remain the same.

4.2. **Canopy Change.** Over the past several decades of recorded daily temperature data at H.J. Andrews Experimental Forest, there has been an observed increase in average annual temperature. To determine whether this increase is a result of global climate change or a direct impact of change in the physical environment, analysis was done using hemispherical photographs. Primarily, the intent was to determine whether there had been a decrease in canopy cover which would allow more direct sunlight, therefore increasing the temperature.

Hemispherical photographs were taken at each of the selected reference stands to capture a 360° view, showing the entire canopy. To determine whether any change in the canopy cover had occurred, photographs from 2001 and 2009 were compared using two different methods. In the first method, the Gap Light Analyzer program was used to calculate percent canopy openness and percent sky area. Using this approach, each photograph was analyzed separately, and then the results were compared, with an increase in canopy openness corresponding to a decrease in canopy cover (see Table 2).

TABLE 2. The percent canopy openness in both 2001 and 2009 for each reference stand, and the inverse change in canopy cover.

Reference Stand	% Canopy Openness 2001	% Canopy Openness 2009	Change in Canopy Cover
2	6.88	5.52	increase
4	7.01	9.82	decrease
5	6.27	9.14	decrease
10	5.24	12.14	decrease
12	4.78	6.16	decrease
20	9.86	4.49	increase
26	9.20	6.91	increase
38	13.88	11.56	increase
86	38.25	28.88	increase
89	8.78	11.61	decrease

In the second approach, a colored 2009 photograph was overlayed onto a black and white 2001 photograph at each reference stand (Figure 6). The following interpretation of the coloration was used:

- black: canopy cover in 2001 but not 2009
- dark color: canopy cover in both 2001 and 2009
- light color: canopy cover in 2009 but not 2001
- white: canopy cover in neither 2001 nor 2009.

For each composition a pixel-count was performed to distinguish between a positive

or negative change in canopy over time. Unfortunately, this method had extremely high sensitivity and therefore yielded unreliable results. Nevertheless, these compositions allow for simple qualitative recognition of canopy change with visual examination.

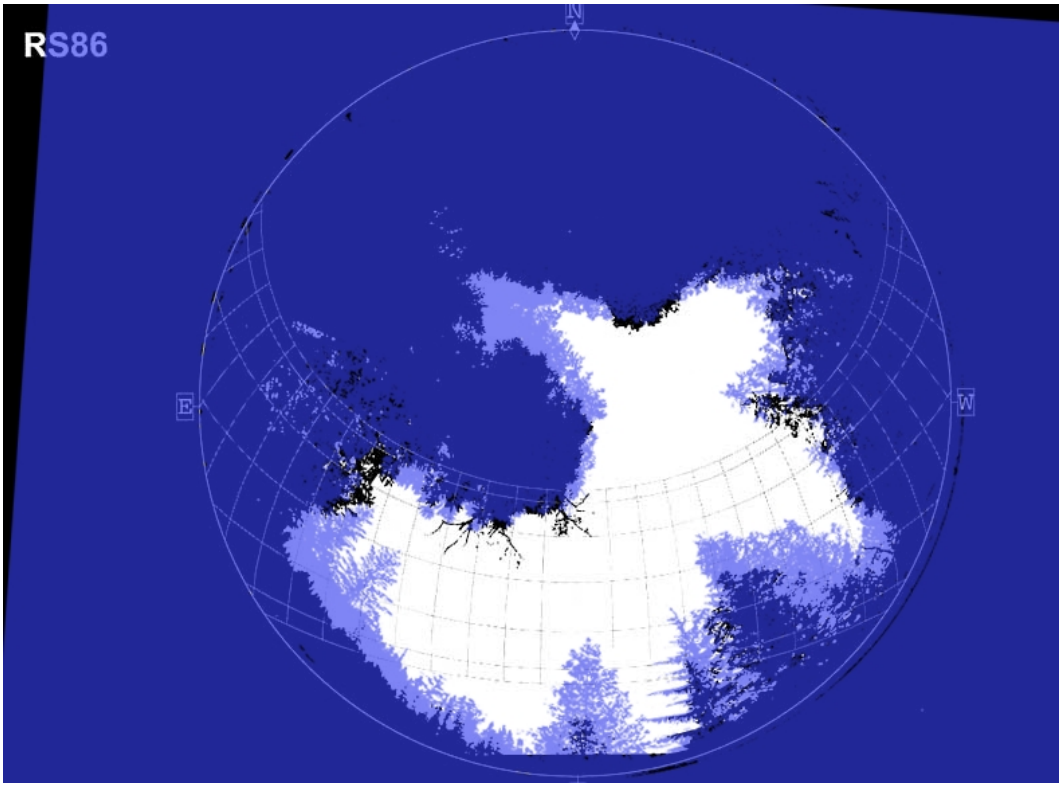

FIGURE 6. Change in canopy cover at Reference Stand 86 showing substantial growth from 2001 to 2009.

From the usable results, it is shown that while half of the reference stands experienced an increase in canopy cover, half experienced a decrease. Since there were no extreme changes which would dramatically increase the amount of direct sunlight and radiation, it is reasonable to conclude that this trend in the H.J. Andrews temperature data may reflect an ongoing change in the global climate. Because, however, these results are not fully conclusive, further analysis is suggested which looks at individual reference stands.

2001 Hemispherical Photographs were taken by Jonathan W. Smith, Oregon State University.

2009 Hemispherical Photographs were taken by Sherri L. Johnson, U.S. Forest Service.

Appendix A. Math of the Transformations

The purpose of this section is to justify the assertions made in Section 4. Section A.1 contains the justification for the position and vector field transformations, while section A.2 presents the justification for the tensor field transformation. Finally, section A.3 proves that the coefficients of spatial distortion are invariant under the transformations.

A.1. **Positions, velocity, and tensor transformations.** Let the frames of reference S_o and S_t, the time parameter t, the unit vectors $\mathbf{e_1}, \mathbf{e_2}, \mathbf{T}$, and $\mathbf{N}$, and the position, velocity and tensor fields $\mathbf{r}, \mathbf{v}$, and J be defined as in Section 4.1.

A.1.1. *Positions.* In order to rewrite a position vector $\mathbf{r}$ in S_o as it is observed in S_t, we first change the position of $\mathbf{r}$ with respect to S_o to the one it would have in a frame centered at $\mathbf{a}(t)$ but oriented as S_o (this is done by simply subtracting $\mathbf{a}(t)$ from $\mathbf{r}$). The next step is to rewrite the transformed $\mathbf{r}$ in terms of the new basis by multiplying it to its corresponding rotational matrix (since both frames are orthonormal).

By defining $S_t(\mathbf{r}) = \mathbf{r}_t$ as the position vector $\mathbf{r}$ as it is observed in S_t, the transformation between positions from S_o to S_t is

$$\mathbf{r}_t = L(t)(\mathbf{r} - \mathbf{a}(t)) = \begin{pmatrix} (\mathbf{r} - \mathbf{a}(t)) \cdot \mathbf{T}(t) \\ (\mathbf{r} - \mathbf{a}(t)) \cdot \mathbf{N}(t) \end{pmatrix}$$

where $L(t) = \begin{pmatrix} \mathbf{e_1} \cdot \mathbf{T}(t) & \mathbf{e_2} \cdot \mathbf{T}(t) \\ \mathbf{e_1} \cdot \mathbf{N}(t) & \mathbf{e_2} \cdot \mathbf{N}(t) \end{pmatrix}$ is the change-of-basis matrix from $\{\mathbf{e_1}, \mathbf{e_2}\}$ to $\{\mathbf{T}(t), \mathbf{N}(t)\}$.

Since $L(t)$ is an orthonormal matrix, its inverse is given by its transpose, namely, $L(t)^{-1} = \begin{pmatrix} \mathbf{e_1} \cdot \mathbf{T}(t) & \mathbf{e_1} \cdot \mathbf{N}(t) \\ \mathbf{e_2} \cdot \mathbf{T}(t) & \mathbf{e_2} \cdot \mathbf{N}(t) \end{pmatrix}$. Furthermore, in order to rewrite a position vector $\mathbf{r}_t$ in S_t as it is observed in S_o,

$$S_o(\mathbf{r}_t) = \mathbf{r} = L(t)^{-1}(\mathbf{r}_t) + \mathbf{a}(t)$$

A.1.2. *Velocity Vector Field.* The velocity vector $\mathbf{v}(\mathbf{r}, t)$ in S_o is similarly rewritten in S_t by first calculating its relative velocity to S_t at each point, by subtracting $\mathbf{a}'(t)$ from $\mathbf{v}(\mathbf{r}, t)$, and then reorienting the frame again using the rotational matrix $L(t)$. By defining $S_t(\mathbf{v}(\mathbf{r}, t)) = \mathbf{v}_t(\mathbf{r}_t)$ as the velocity vector $\mathbf{v}(\mathbf{r}, t)$ as observed in S_t,

$$\mathbf{v}_t(\mathbf{r}_t) = L(s)(\mathbf{v}(\mathbf{r}, t)) - \mathbf{a}'(t))$$

Similarly, In order to express a velocity $\mathbf{v}_t(\mathbf{r}_t)$ in S_t as it is observed in S_o,

$$S_o(\mathbf{v}_t(\mathbf{r}_t)) = \mathbf{v}(\mathbf{r}, t) = L(t)^{-1}(\mathbf{v}_t(\mathbf{r}_t)) + \mathbf{a}'(t)$$

A.1.3. *Velocity Gradient Tensor Field.* The tensor field $J(\mathbf{r},t)$ can now be rewritten as it is observed in S_t by calculating it from the new vector field $S_t(\mathbf{v}(\mathbf{r},t))$:

$$S_t(J(\mathbf{r},t)) = J_t(\mathbf{r}_t) = \nabla_t \otimes \mathbf{v}_t(\mathbf{r}_t)$$

where $\nabla_t = \frac{\partial}{\partial \mathbf{T}(t)}\mathbf{T}(t) + \frac{\partial}{\partial \mathbf{N}(t)}\mathbf{N}(t)$ and '$\otimes$' is the tensor product. Nevertheless, calculating $J_t(\mathbf{r}_t)$ can be simplified by using the following transformation:

$$J_t(\mathbf{r}_t) = L(t)J(\mathbf{r},t)L(t)^{-1}$$

Section A.2 presents a proof that this transformation is valid for any tensor field $J(\mathbf{r},t)$.

A.2. **Proof of Tensor Transformation Formula.** The tensor $J_t(\mathbf{r}_t)$ in S_t is given by

$$J_t(\mathbf{r}_t) = \nabla_t \otimes \mathbf{v}_t(\mathbf{r}_t) = \begin{pmatrix} \partial_{\mathbf{T}(t)}(\mathbf{v}_t(\mathbf{r}_t)\cdot\mathbf{T}(t)) & \partial_{\mathbf{N}(t)}(\mathbf{v}_t(\mathbf{r}_t)\cdot\mathbf{T}(t)) \\ \partial_{\mathbf{T}(t)}(\mathbf{v}_t(\mathbf{r}_t)\cdot\mathbf{N}(t)) & \partial_{\mathbf{N}(t)}(\mathbf{v}_t(\mathbf{r}_t)\cdot\mathbf{N}(t)) \end{pmatrix}$$

The claim is that $J_t(\mathbf{r}_t) = L(t)J(\mathbf{r},t)L(t)^{-1}$, which we will prove by showing the equivalence of $L(t)J(\mathbf{r},t)L(t)^{-1}$ to $J_t(\mathbf{r}_t)$.

The product $L(t)J(\mathbf{r},t)L(t)^{-1} = LJL^{-1}$ is given by

$$\begin{pmatrix} \mathbf{e_1}\cdot\mathbf{T}(t) & \mathbf{e_2}\cdot\mathbf{T}(t) \\ \mathbf{e_1}\cdot\mathbf{N}(t) & \mathbf{e_2}\cdot\mathbf{N}(t) \end{pmatrix} \begin{pmatrix} \partial v_1(\mathbf{r},t)/\partial\mathbf{e_1} & \partial v_1(\mathbf{r},t)/\partial\mathbf{e_2} \\ \partial v_2(\mathbf{r},t)/\partial\mathbf{e_1} & \partial v_2(\mathbf{r},t)/\partial\mathbf{e_2} \end{pmatrix} \begin{pmatrix} \mathbf{e_1}\cdot\mathbf{T}(t) & \mathbf{e_1}\cdot\mathbf{N}(t) \\ \mathbf{e_2}\cdot\mathbf{T}(t) & \mathbf{e_2}\cdot\mathbf{N}(t) \end{pmatrix}$$

which can be written more compactly as

$$= \begin{pmatrix} T_1 & T_2 \\ N_1 & N_2 \end{pmatrix} \begin{pmatrix} \partial_{e1}v_1 & \partial_{e2}v_1 \\ \partial_{e1}v_2 & \partial_{e2}v_2 \end{pmatrix} \begin{pmatrix} T_1 & N_1 \\ T_2 & N_2 \end{pmatrix}$$

matrix multiplication shows that the resulting matrix M has as components:

$$M_{i,j} = L_{j,1}[L_{i,1}\partial_{e1}v_1 + L_{i,2}\partial_{e1}v_2] + L_{j,2}[L_{i,1}\partial_{e2}v_1 + L_{i,2}\partial_{e2}v_2]$$

where $i,j \in \{1,2\}$. The components can be rewritten as

$$M_{i,j} = L_{i,1}[L_{j,1}\partial_{e1}v_1 + L_{j,2}\partial_{e2}v_1] + L_{i,2}[L_{j,1}\partial_{e1}v_2 + L_{j,2}\partial_{e2}v_2]$$

Recalling that the directional derivative in a direction $\mathbf{u} \in \mathbb{R}^2$ of a function $f(x,y) : \mathbb{R}^2 \to \mathbb{R}$ is given by $\partial_{\mathbf{u}}f(x,y) = (\mathbf{e_1}\cdot\mathbf{u})\partial_{e1}f(x,y) + (\mathbf{e_2}\cdot\mathbf{u})\partial_{e2}f(x,y)$, M is rewritten as

$$M_{i,j} = L_{i,1}\partial_{u_j}v_1 + L_{i,2}\partial_{u_j}v_2 = \partial_{u_j}(L_{i,1}v_1 + L_{i,2}v_2)$$

where $u_1 = \mathbf{T}$ and $u_1 = \mathbf{N}$.

But $(L_{i,1}v_1 + L_{i,2}v_2) = (L\cdot\mathbf{v})_i$ as it can be seen by performing the matrix multiplication. Furthermore, $\partial_{u_j}(L\cdot\mathbf{a}(\mathbf{t}))_i = 0$ because $L\cdot\mathbf{a}(\mathbf{t})$ is the same at all points in space, meaning that

$$M_{i,j} = \partial_{u_j}(L\cdot\mathbf{v})_i = \partial_{u_j}[(L\cdot\mathbf{v})_i + (L\cdot\mathbf{a}(\mathbf{t}))_i] = \partial_{u_j}(L\cdot(\mathbf{v}+\mathbf{a}(\mathbf{t})))_i$$

Since $\mathbf{v}_t(\mathbf{r}_t) = L\cdot(\mathbf{v}+\mathbf{a}(\mathbf{t}))$, the components can now be rewritten as $M_{i,j} = \partial_{u_j}\mathbf{v}_t(\mathbf{r}_t)_i = \partial_{u_j}(\mathbf{v}_t(\mathbf{r}_t)\cdot\mathbf{u_j})$ and the matrix $M = LJL^{-1}$ becomes

$$LJL^{-1} = \begin{pmatrix} \partial_{\mathbf{T}(t)}(\mathbf{v}_t(\mathbf{r}_t)\cdot\mathbf{T}(t)) & \partial_{\mathbf{N}(t)}(\mathbf{v}_t(\mathbf{r}_t)\cdot\mathbf{T}(t)) \\ \partial_{\mathbf{T}(t)}(\mathbf{v}_t(\mathbf{r}_t)\cdot\mathbf{N}(t)) & \partial_{\mathbf{N}(t)}(\mathbf{v}_t(\mathbf{r}_t)\cdot\mathbf{N}(t)) \end{pmatrix} = J_t(\mathbf{r}_t)$$

proving our claim.

A.3. **Distortion coefficients invariance.** The components of a tensor J_t observed in S_t are given by

$$(J_t)_{i,j} = L_{j,1}[L_{i,1}\partial_{e1}v_1 + L_{i,2}\partial_{e1}v_2] + L_{j,2}[L_{i,1}\partial_{e2}v_1 + L_{i,2}\partial_{e2}v_2]$$

Given the fact that $N_1 = -T_2$, $N_2 = T_1$, and $T_1^2 + T_2^2 = 1$, the expressions for the distortion coefficients can be greatly simplified (this would have not been the case if a non-orthonormal basis for S_t were to be chosen).

The coefficient of isotropic expansion $(\gamma_d)_t$ observed in S_t is

$$\begin{aligned}
(\gamma_d)_t &= [(J_t)_{1,1} + (J_t)_{2,2}]/2 \\
&= [T_1(T_1J_{1,1} + T_2J_{2,1}) + T_2(T_1J_{1,2} + T_2J_{2,2})]/2 \\
&\quad + [N_1(N_1J_{1,1} + N_2J_{2,1}) + N_2(N_1J_{1,2} + N_2J_{2,2})]/2 \\
&= [(T_1^2 + N_1^2)J_{1,1} + (T_1T_2 + N_1N_2)(J_{2,1} + J_{1,2}) + (T_2^2 + N_2^2)J_{2,2}]/2 \\
&= [(T_1^2 + (-T_2)^2)J_{1,1} + (T_1T_2 + (-T_2)(T_1))(J_{2,1} + J_{1,2}) + (T_2^2 + (T_1)^2)J_{2,2}]/2 \\
&= [J_{1,1} + J_{2,2}]/2 \\
&= \gamma_d
\end{aligned}$$

Similarly, the coefficient of isotropic rotation $(\gamma_r)_t$ observed in S_t is

$$\begin{aligned}
(\gamma_r)_t &= [(J_t)_{2,1} + (J_t)_{1,2}]/2 \\
&= [T_1(N_1J_{1,1} + N_2J_{2,1}) + T_2(N_1J_{1,2} + N_2J_{2,2})]/2 \\
&\quad - [N_1(T_1J_{1,1} + T_2J_{2,1}) + N_2(T_1J_{1,2} + T_2J_{2,2})]/2 \\
&= [(T_1N_2 - T_2N_1)J_{2,1} + (T_2N_1 - T_1N_2)J_{1,2}]/2 \\
&= [(T_1(T_1) - T_2(-T_2))J_{2,1} + (T_2(-T_2) - T_1(T_1))J_{1,2}]/2 \\
&= [J_{2,1} - J_{1,2}]/2 \\
&= \gamma_r
\end{aligned}$$

A little more algebra shows that, for the coefficient of anisotropic expansion $(\gamma_s)_t$ observed in S_t,

$$(J_t)_{1,1} - (J_t)_{2,2} = (J_{1,1} - J_{2,2})(T_1^2 - T_2^2) + 2T_1T_2(J_{2,1} + J_{1,2}),$$

$$(J_t)_{1,2} + (J_t)_{2,1} = (J_{2,1} + J_{1,2})(T_1^2 - T_2^2) + 2T_1T_2(J_{2,2} - J_{1,1})$$

and finally

$$\begin{aligned}
&((J_t)_{1,1} - (J_t)_{2,2})^2 + ((J_t)_{1,2} + (J_t)_{2,1})^2 \\
&\qquad = (T_1^2 - T_2^2)^2((J_{1,1} - J_{2,2})^2 + (J_{2,1} + J_{2,2})^2) + 4T_1^2T_2^2((J_{2,1} + J_{1,2})^2 + (J_{2,2} - J_{1,1})^2) \\
&\qquad = (T_1^4 + 2T_1^2T_2^2 + T_2^4)((J_{1,1} - J_{2,2})^2 + (J_{2,1} + J_{2,2})^2) \\
&\qquad = (T_1^2 + T_2^2)^2((J_{1,1} - J_{2,2})^2 + (J_{2,1} + J_{2,2})^2) \\
&\qquad = (J_{1,1} - J_{2,2})^2 + (J_{1,2} + J_{2,1})^2
\end{aligned}$$

implying that $(\gamma_s)_t = \gamma_s$

Since the three distortion coefficients are the same after the transformation, the difference between $J_t(\mathbf{r}_t)$ and $J(\mathbf{r}, t)$ must lie in the angle of anisotropic scaling θ. In S_o, it is given by $\theta = \text{Angle}\{\binom{J_{1,1}-J_{2,2}}{J_{1,2}+J_{2,1}}\}$, while in S_t it becomes

$$\theta_t = \text{Angle}\left\{\begin{pmatrix}(J_t)_{1,1} - (J_t)_{2,2}\\(J_t)_{1,2} + (J_t)_{2,1}\end{pmatrix}\right\} = \text{Angle}\left\{\begin{pmatrix}(J_{1,1} - J_{2,2})(T_1^2 - T_2^2) + 2T_1T_2(J_{2,1} + J_{1,2})\\(J_{2,1} + J_{1,2})(T_1^2 - T_2^2) + 2T_1T_2(J_{2,2} - J_{1,1})\end{pmatrix}\right\}$$

Acknowledgments

We are very thankful to those who made our research experience possible: The EISI Program Director, Desiree Tullos, our advisors Julia Allen Jones, Eugene Zhang, and Jonathan Palacios, and our math tutor Jorge Ramirez.

We are grateful for funding through the NSF grant DMS-0609356.

References

[1] Eugene Zhang, Harry Yeh, Zhongzang Lin, Robert S. Laramee, "Asymmetric Tensor Analysis for Flow Visualization," IEEE Transactions on Visualization and Computer Graphics, vol. 15, no. 1, pp. 106-122, Jan./Feb. 2009, doi:10.1109/TVCG.2008.68

[2] Perkins, R.M. and J.A. Jones. In press. Climate variability, snow and physiographic controls on storm hydrographs in small forested basins, western Cascades, Oregon. Hydrological Processes.

[3] Weickert and Hagen, 2005 In: J. Weickert and H. Hagen, Editors, Visualization and Processing of Tensor Fields, Springer (2005)